Two Different Strategies for Palladium Reduction on Spinel $ZnMn_2O_4$ Micro-Sponge: Application in the Electrochemical Oxidation of Formaldehyde

Yavari, Zahra*•*+; Kaedi, Fariba
Department of Chemistry, Faculty of Basic Sciences,
University of Sistan and Baluchestan, Zahedan, I.R. IRAN

Farrokhi, Mojtaba; Abbasian, Ahmad Reza
Department of Materials Engineering, Faculty of Engineering,
University of Sistan and Baluchestan, Zahedan, I.R. IRAN

ABSTRACT: *The formaldehyde, HCHO, is generated via the partial oxidation of methanol, and the investigation of its electrochemical oxidation is essential for the complete knowledge of methanol oxidation. Ceramic material with a spongy structure can promote the dispersion of noble metals as the main catalyst for the electrooxidation of organic molecules. In this research, spinel $ZnMn_2O_4$ (ZMO) micro-sponge was synthesized, characterized, and utilized as a booster for the Pd catalyst. Palladium was stabilized on ZMO with two different strategies, containing reduction with sodium borohydride and zinc plate. The samples were assessed using X-ray diffraction, scanning electron microscopy, transition electron microscopy, and electrochemistry. In comparison with non-promoted Pd, Pd/ZMO electrocatalyst showed excellent efficiency in parameters like electrochemical active surface area and turnover parameters. The outcomes represented that the palladium nanoparticles are reduced with the chemical system having a lesser diameter and better dispersion than the electrochemical one. Consequently, as we expected, the electrochemical oxidation of formaldehyde showed better results for the reduction by the chemical in comparison with electrochemical reduction systems.*

KEYWORDS: *Formaldehyde oxidation; $NaBH_4$; Reduction Sstrategy; Spinel $ZnMn_2O_4$ micro-sponge; Zn/HCl system.*

INTRODUCTION

Despite the dangers of using formaldehyde (HCHO), it is unexpected to leave this material in different industries. So always, the oxidation of HCHO has been studied in many fields as a result of (i) unwanted side effects on the human body in electrochemical sensors [1, 2], (ii) pollutants eliminated by converting to O_2 and H_2O [3, 4], (iii) facility to lessen the electrodeless metals deposition [5], and,

**To whom correspondence should be addressed.*
+ E-mail: zahrayavari5@gmail.com
• Other Address: Renewable Energies Research Institute, University of Sistan and Baluchestan, Zahedan, I.R. IRAN
1021-9986/2023/9/2920-2932 14/$/6.04

(iv) providing high current in the polymer electrolyte membrane fuel cells as an electron donor [2, 6, 7]. The HCHO is generated *via* the partial oxidation of methanol, and the investigation of its electrooxidation is essential for the complete knowledge of methanol oxidation. Hence, HCHO electrooxidation as a heterogeneous reaction is frequently utilized to entirely comprehend the electrochemical processes and the performance study of electrocatalysts [8, 9]. The heterogeneous electrocatalysts have great recyclability, high enduring, easy immobilization, and successful electrode integration. They often have low efficiency because of the limited active centers on the surface of the reactants. High surface area and required active sites can be available for an effective electrocatalysis process with highly dispersed metal nanostructures on the electrode surface. Numerous electrocatalysts are reported for HCHO electrochemical oxidation including the Fe3O4@Pt core-shell nanoparticles/carbon-ceramic electrode [10], nano-Pd on iodized carbon nanotubes [11], nano-Pd on carbon ionic liquid composite [12], Au nanoparticles [13], Pt–Pd on polypyrrole multi-walled carbon nanotubes [14], Fe^{2+}-nano-zeolite [7], nanostructured silver [6], Ni^{2+} dispersed onto chitosan [15], and composites containing nickel [16], and copper [17].

Pd-based structures are known as efficient catalysts for the electrochemical oxidation of small fuels [18, 19] like HCHO. Producing noble metal catalysts with high purity, significant surface area, low load, and long life has always been a technological challenge. The Pd-based electrocatalysts are made by a chemical or electrochemical reduction.

In 2022, *Altuner et al*, used palladium-carbon nanoparticles as the alternative to the biologically used horseradish peroxidase enzyme to release tetramethylbenzidine in the presence of phosphate ions. Thus, they presented a protein-independent phosphate sensor [20].

The chemical reduction involves the gaining electrons by Pd^{2+} ions through a reducing agent such as glycerol [21], sodium borohydride [22], CO gas [23], electrons generated by high-energy radiations [24], adsorbed OH^- on hematite [25], etc.

The binary and ternary catalysts based on palladium, which increase the catalytic activity of this noble metal, also cause its durability [26, 27]. Nano-sized promoters and supports can be effective in this case; because they restrain the agglomerating palladium, and form a stable structure with high surface area, capably; with having the encouraging electronic and geometric properties to advance the interaction among particles of noble metals and surface, resulting in the upgrading catalytic activity [28]. Therefore, the materials with similar composition and different morphologies have been studied [29-31].

The oxides containing transition metal proliferate as the promotor [18, 32], and catalytic component [33] for electrochemical oxidation reactions. Including attractive aspects of these oxides are complex ion formation, variable oxidation state, and catalytic performance. Adsorption of HCHO on the surface of intermediate metal electrocatalysts improves the oxidation process of HCHO. In this process, the creation of CHO_{ads} is a vital agent for dehydrogenation to desorb CO_2 from the electrocatalyst surface [34].

Mesoporous metal oxides are attractive, owning to structural characteristics. They are utilized as proper supports or electrocatalysts in heterogeneous electrocatalysis for bulkier molecules. These supports provide transport ions and electrons by a shorter pathway, and it will result in rapid process kinetics [22]. Spinel-type manganese oxides have revealed multiple valences, inherent magnetic and optical properties, various arrangements, chemical properties, and superb electron configurations [35]. $ZnMn_2O_4$ belongs to normal spinels, and is nontoxicity, has a high theoretical capacity, and low price [36]. Researchers have reported numerous scientific methods for the fabrication of this spinel oxide, including hydrothermal [37], sol-gel [38], solid-state reaction [39], solvothermal [40], co-precipitation [41], and polymer pyrolysis [42]. The Pechini-type sol-gel auto-combustion is a suitable route for successfully synthesizing oxides, which acts based on a reaction between the fuel and the complexing agent [43]. Pechini method is interesting due to the simple control, high speed, low temperature, availability and affordability of the apparatus, low price and toxicity of reagents, pH adjustment, and the chance of industrialization [44]. Several modifying agents can act as ligands and reactants in this route [45, 46]. The utilization benefit of citric acid and glycol as fuel and complexing mediators involves a homogeneous combining numerous metallic ions at the atomic level to a single arrangement phase, pure and too ordered porous oxide structures

with remarkable configurations during the production process [47].

Three goals are pursued in the current research: (I) Enhancing the electrocatalytic behavior of palladium using $ZnMn_2O_4$ (ZMO); (II) Comparison of the chemical and electrochemical reduction of palladium; and (III) Comparing the performance of the ZMO/Pd nanoparticles towards HCHO electrochemical oxidation *via* electrochemical techniques.

EXPERIMENTAL SECTION

Materials

Zinc nitrate hexahydrate (CAS No: 10196-18-6), Manganese (II) nitrate tetrahydrate (20694-39-7), 99.5%citric acid monohydrate (5949-29-1), ethylene glycol (107-21-1), 37% hydrochloric acid (7647-01-0), 99% acetic acid (64-19-7), sodium borohydride (16940-66-2), and 97% sulfuric acid (7664-93-9) were purchased from Merck Company without any purification were used in this research. Palladium chloride (7647-10-1) and medium molecular weight chitosan (9012-76-4) were purchased from Sigma-Aldrich and Fluka Companies, respectively.

Instrumentation

The crystalline phase of the sample was recognized by X-Ray Diffraction (XRD, Bruker D8 Advance) operated at 40 keV and 30 mA with Cu kα radiation of wavelength λ= 1.5418Å. The surface morphology was investigated by KYKY Scanning Electron Microscope (SEM) Model EM3900M. Field emission scanning electron microscopy (FESEM, SAMX electron microscope MIRA3 TESCAN) was used to detect as-acquired samples. The TEM micrographs were obtained using a Philips CM120 transmission electron microscope. It used an auto-lab PGSTAT 128N (EcoChemie, Netherlands) potentiostat/galvanostat having Hg/HgO, Pt, and glassy carbon electrodes.

Synthetization of ZMO

To synthesize the spinel oxide, 0.01 mol of $Zn(NO_3)_2.6H_2O$ and 0.02 mol of $Mn(NO_3)_2.4H_2O$ were dissolved in 100 mL deionized water resistivity of 18.0 MΩ.cm produced through a Milli-Q purifier and mixed for 30 min at laboratory temperature. Then, 0.024 mol of citric acid $HO_2C\text{-}CH_2\text{-}C(HO)(HO_2C)\ HO_2C$ was incorporated with the above solution and stirred for 30 min. The temperature was enhanced to 70 ˚C, and 0.012 mol of ethylene Glycol $(CH_2OH)_2$ was added to the system. The viscosity of the solution graduates increased due to gel formation. The temperature rose to 200 ˚C. Afterward, the gel was suddenly ignited and turned to gray powder. The powder was calcined at 700 ˚C to get spinel oxide.

Pd loading on ZMO

1% (weight/volume) chitosan (a derivative of chitin) solution was prepared in 1% (volume/volume) acetic acid aqueous solution. The as-prepared suspension was mixed to dissolve, kept for 24 h, and filtered before use to remove any impurities. Due to its large molecular weight, chitosan acts as an important support material for catalysts in catalytic reactions [48].

Palladium was loaded on the ZMO sample with two different systems. In the first strategy (chemical system): 3 mg ZMO was mixed with 1 mL of chitosan solution, and followed by sonication until getting a uniform ink.

In a typical method for the preparation of Pd nanoparticles, in another container, 5 mg $PdCl_2$ was mixed with 1 mL double distillation water. 20 µL 37% HCl solution was added to improve the dissolution by converting Pd^{2+} to Pd^{4+} and creating a soluble complex. 2 mL chitosan solution was added as the binder agent. The containers' contents were mixed. The suspension was stirred overnight to load palladium ions on the surface and inside cavities of oxide support. To synthesize Pd nanoparticles, palladium ions were reduced chemically with $NaBH_4$. To achieve complete reduction, $NaBH_4$ concentration was 5 times more than Pd concentration. $NaBH_4$ solution was added to the mixture, and stirred for 1 h.

The glassy carbon electrode with a radius of 1 mm was polished with Al_2O_3 slurry. The procedure was followed by sonication in 3:1 water and ethanol mixture for about 5 min. The activating process of the cleaned electrode was continued by sweeping potential between -1.5 and +1.5 V in acidic media until a stable cycle. Finally, 5 µL

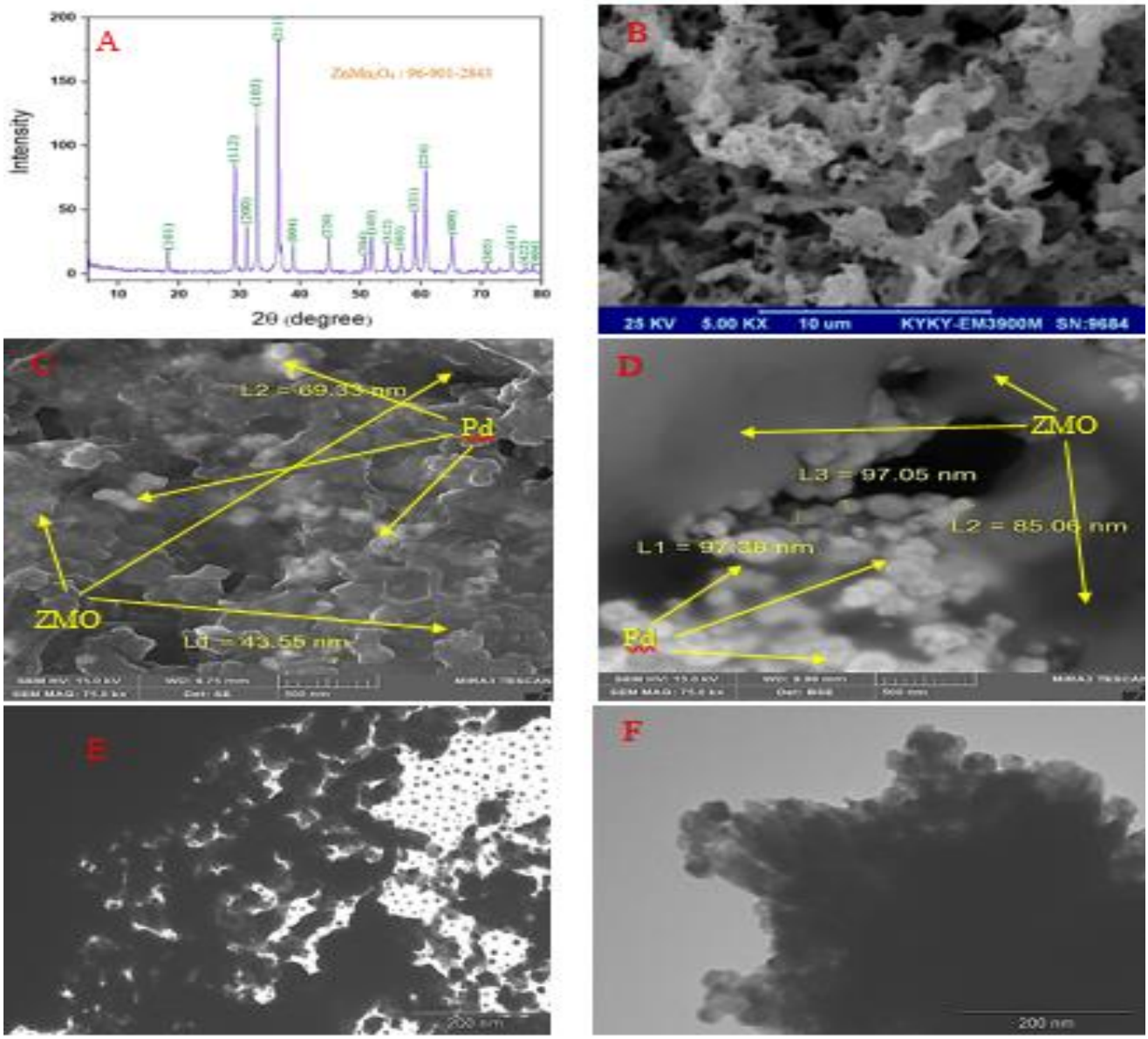

Fig. 1: (A) The XRD pattern, (B) the SEM image of the synthesized ZMO, (C) FESEM image of the Pd_{rNBH}/ZMO, (D) FESEM image of the Pd_{rZHC}/ZMO, (E) TEM image of Pd_{rNBH}/ZMO, and (F) TEM image of Pd_{rZHC}/ZMO

of the composite containing chemically reduced Pd on ZMO surface was put by micropipette onto the prepared electrode. Evaporation of the solvent created a catalytic layer on the surface of the electrode and its modification. The second layer was applied to improve the loading by placing the next 5 µL. The as-modified electrode was symbolized as Pd_{rNBH}/ZMO. For comparison, non-promoted Pd was synthesized according to the 1st strategy, and denoted as Pd_{rNBH}.

Another strategy is spontaneous reduction, which happens in an electrochemical galvanic cell. 7 µL mixture of 3 mg ZMO + 50 µL 37% HCl + 2 mL distilled H_2O + 5 mg $PdCl_2$ + 4 mL chitosan solution 2 mg/L in 1% acetic acid was dropped on a glassy carbon electrode (activated as described above). In succeeding, the reduction of Pd ions (Pd^{2+}) coincided with transferring two electrons from a zinc plate as an anode to the acquired electrode as a cathode by immersing in into an acidic solution (5wt % HCl) for 10 s. The as-modified electrode was labeled as Pd_{rZHC}/ZMO. Pd_{rZHC} was synthesized according to the 2nd strategy. The Pd loading in all modified electrocatalysts was 0.310 mg/cm^2.

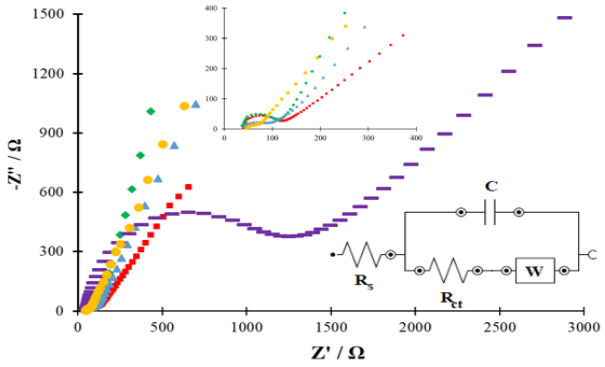

Fig. 2: Nyquist plots (Inset: Equivalent Circuit) for (—: dash) bare glassy carbon electrode, and electrocatalysts of (♦: diamond) Pd_{rNBH}, (●: circle) Pd_{rNBH}/ZMO, (■: square) Pd_{rZHC} and (▲: triangle) Pd_{rZHC}/ZMO

RESULTS AND DISCUSSION

Characterization

Fig.1A is the XRD pattern of the ZMO sample. The diffraction peaks of the sample come from the reflections of $ZnMn_2O_4$ according to the 96-901-2843 reference code. Its crystal system is a tetragonal I 41/a m d space group. The sol-gel auto-combustion is an exothermic process and is usually applied to synthesize nanosized oxides [49]. In this process, the metal nitrates and organic matter fuel (herein citric acid and ethylene glycol) react together. The nitrate ions act as the oxidants and the fuels as the reducing agent [50]. During the combustion process, some gases are produced according to the following reactions, and the metal oxides will be formed simultaneously. The release of gaseous through the sample during the ignition caused porous structure matter according to Eq. (1), as observed in SEM images (Fig. 1B).

$$Zn(NO_3)_2 + 2\,Mn(NO_3)_2 + 2.4\,C_6H_8O_7 + 1.2\,C_2H_6O_2 + 13.4\,O_2 \rightarrow ZnMn_2O_4 + 16.8\,CO_2\uparrow + 13.2\,H_2O\uparrow + 3\,N_2\uparrow \quad (1)$$

Since the acquired xerogel burns when heated at moderately low temperatures, this method is named the sol-gel auto-combustion. The environment-friendly process to achieve pure homogenous fine particles, lacking requiring complicated apparatus or high-cost precursors, low operating temperature, and control over the end stoichiometry are the main benefits of this method.

Comparative analysis of two Pd synthesis systems helps predict the Pd state from the point of view of purity and morphology. The standard reduction voltage of Pd is:

$$Pd^{2+}_{(aq)} + 2\,e^- \rightarrow Pd_{(s)}\downarrow \qquad \text{in } +0.91\ (V) \quad (2)$$

In 1st strategy, $NaBH_4$ is decomposed in solution and formed hydride ions:

$$NaBH_4 \rightarrow Na^+ + H^- + BH_3\ (\text{or } B_2H_6) \quad (3)$$

And then, the electrons are supplied as follows:

$$2\,H^-_{(aq)} \rightarrow H_{2(g)}\uparrow + 2\,e^- \qquad \text{in } +2.23\ (V) \quad (4)$$

And in 2nd strategy:

$$Zn_{(s)} \rightarrow Zn^{2+}_{(aq)} + 2\,e^- \qquad \text{in } +0.76\ (V) \quad (5)$$

The more voltage of the cell in the chemical system than the electrochemical one evinces big changes in Gibbs free energy.

The status of Pd_{rZHC}/ZMO and Pd_{rNBH}/ZMO samples were probed by FESEM, demonstrated in Figs. 1C and 1D. It is seen in the entrance of palladium onto the surface and into ZMO pores. The palladium dispersion occurred on the oxide support. Comparing two micrographs, the palladium is synthesized with a lesser diameter and better dispersion in the 1st strategy than in the other. The chemical reduction was carried out in the liquid phase, whereas palladium ions were present, and the ZMO was dispersed there.

In contrast, the electrochemical reduction was made on the surface of the electrode; and the species mobility was more limited. So, less polarization was presumably happened in 1st strategy, and the process kinetics would be faster. Also, TEM was used to characterize Pd_{rNBH}/ZMO and Pd_{rZHC}/ZMO, and the results were shown in Figs. 1E and F, respectively. The TEM for Pd_{rNBH}/ZMO shows the palladium particles being finer and having more cavities in the electrocatalyst structure than the Pd_{rZHC}/ZMO. It can make the former perform better than the latter. In 2018, Eshghi and his colleagues synthesized Pt-Fe/rGO via chemical reduction with $NaBH_4$ and compared its performance for methanol oxidation with an electrodeposited Pt/Al catalyst. Their data showed the superiority of chemical reduction over electrochemical [51].

Electrochemical studies

The Nyquist plots were exhibited for the bare glassy carbon electrode, and electrocatalysts of Pd_{rNBH}, Pd_{rNBH}/ZMO, Pd_{rZHC}, and Pd_{rZHC}/ZMO in Fig. 2. According to the outcomes, the equivalent circuit is defined as $R_s(C[R_{ct}W])$, wherein R_s, R_{ct}, C, and W were medium resistance, charge transfer resistance double-layer capacitance, and Warburg impedance, respectively.

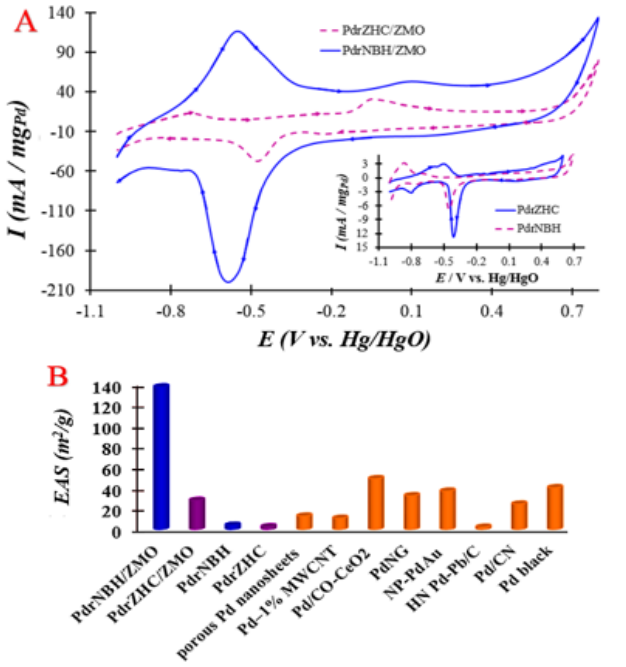

Fig. 3: (A) The CV curves of the synthesized modified electrocatalysts in 1 M NaOH solution and (B) Comparison of EAS bar charts in this work and literature

The R_{ct} was 1005 Ω for bare glassy carbon electrode, 66.5 Ω for Pd_{rZHC}, 56.1 Ω for Pd_{rNBH}, 44.9 Ω for Pd_{rZHC}/ZMO and 25.4 Ω for Pd_{rNBH}/ZMO. The decrease in R_{ct} implies higher conductivity of the electrode surface. A comparison of data showed that the method of palladium reduction and the presence of support in the electrocatalyst could affect the conductivity of the electrode surface by changing the palladium dispersion. Therefore, it is predicted that the use of a strong reductant compared to electrochemical reduction will make Palladium perform better as an electrocatalyst.

To show the potential efficiency, the electrochemical properties of the as-modified electrodes were measured in alkali media. Fig. 3A reveals CVs of Pd_{rNBH}/ZMO, Pd_{rZHC}/ZMO, Pd_{rNBH}, and Pd_{rZHC} electrocatalysts in the caustic soda solution. The positive-going sweep directed an electrochemical oxidation reaction on the electrode surface, followed by the hydrogen desorption and creation of Pd oxides; at the same time, the negative-going scan resulted from the reduction of the Pd oxides and hydrogen adsorption (eq. 6 and eq.7) [52, 53]:

$$Pd\text{-}H_{ads/des} + OH^- \rightarrow Pd + H_2O + e^- \quad (6)$$

$$Pd\text{–}O + H_2O + 2e^- \rightarrow Pd + 2OH^- \quad (7)$$

As it clears in Fig. 3A, the large surface in the adsorption/desorption of hydrogen peaks and the PdO formation/reduction peaks in the Pd_{rNBH}/ZMO electrocatalyst demonstrated the Pd_{rNBH}/ZMO electrocatalyst has a farther Electrochemical Active Surface (EAS) area. The EAS of Pd nanoparticles for every four electrocatalysts has been acquired by integrating the reduction of PdO and adsorption/desorption of hydrogen peaks based on [54, 55]. To comparison of EAS in this work and other electrocatalysts containing Pd, such as porous Pd nano-sheets [56], Pd-5% multi-walled carbon nanotube [67], Pd/CO-CeO_2 [47], Pd nanoparticles were deposited on nitrogen-doped graphene (PdNG) [58], Nanoporous-PdAu [59], hallow nano-spheres Pd-Pb/C [60], Pd/carbon nano-foam [61] and Pd black [62], the EAS bar chart is designed and presented in Fig. 3B. The presence of many available active sites on the surface of electrocatalysts brings about having large EAS. As observed in Fig. 3A and B, utilizing a 3D porous and spongy composite (ZMO) as support for Pd electrocatalyst enhanced EAS of modified electrodes, which can be attributed to the synergistic influences, for instance bifunctional, electronic, and geometry of ZMO composite. In addition, about supported nanoparticles, an ultra-thin surface ZMO support arrangement before the onset of bulk oxidation. This thin surface oxide is more active under oxidation conditions [63].

The Pd's distribution in each electrocatalyst has been estimated according to previous work [56] ($D \times 10^{-2} = 6.19$ for Pd_{rNBH}/ZMO, 1.08 for Pd_{rZHC}/ZMO, 0.18 Pd_{rNBH}, and 0.11 for Pd_{rZHC}). To have a better comparison, the calculated electrochemical data are collected in Table 1.

The ability of HCHO oxidation was studied on supported electrocatalysts in 1 M NaOH + 0.26 M HCHO solution with 50 mV/s rate and was compared with support-less ones (Fig. 4A). The shoulder at about 0.4 V, can be attributed multi-steps oxidation of formaldehyde. the voltammograms of electrooxidation for light organic compounds such as alcohols, aldehydes, and carboxylic acids have an unexpected behavior in reverse scan. So that during the cyclic scan, anodic peaks are always observed and the reduction process does not occur on surface of working electrodes. This is due to the nature of the multi-step and irreversible of oxidation of these compounds. In reverse scan, intermediates produced in partial oxidation during forward scan can be oxidized. These intermediates include $Pd(COOH)_{ads}$ and $Pd(CO)_{ads}$ (please, see Eq. (8)).

Table 2: The comparison of electrochemical data toward HCHO oxidation on modified electrodes in this work and some other electrocatalysts

Electrocatalyst	Electrolyte	[HCHO] (M)	Current density	Sweep rate ($mV.s^{-1}$)	Ref.
Pd/C	0.1M NaOH	0.10	103 mA/mg_{Pd}	50	[64]
$Pd/TiO_2NT/Ti$	0.1 M NaOH	0.05	20.40 mA/cm^2	100	[65]
GO-BDMA-Pd	1.0 M NaOH	0.10	50.24 mA/cm^2	50	[66]
Nanoporous silver	0.9 M KOH	0.3	35 mA/cm^2	20	[67]
Ag nanoprisms	1.0 M NaOH	0.1	4.5 mA/cm^2	50	[68]
Pd-NP/EG-MWCNT	1.0 M KOH	0.05	0.47 mA	100	[69]
MWCNTs/Pt	0.5 MH_2SO_4	1.00	84.74 mA/mg_{Pt}	50	[7۰]
graphene–MWCNTs/Pt			241.14 mA/mg_{Pt}		
Pd_{rZHC}/ZMO	1.0 M NaOH	0.26	120.21 mA/mg_{Pd}	50	This work
Pd_{rNBH}/ZMO			420.89 mA/mg_{Pd}		
Pd_{rNBH}			35.23 mA/mg_{Pd}		
Pd_{Rzhc}			21.13 mA/mg_{Pd}		

The electron released from these compounds increases the current in the reverse scan. As can see in Fig. 4A, the anodic current of HCHO oxidation over the Pd_{rNBH}/ZMO electrocatalyst fully advanced at 420.89 mA/mg_{Pd} was much higher than Pd_{rZHC}/ZMO (= 120.21 mA/mg_{Pd}), Pd_{rNBH} (=35.23 mA/mg_{Pd}), and Pd_{rZHC} (=21.13 mA/mg_{Pd}) electrocatalysts. This data is comparable with other electrocatalysts for HCHO oxidation (see Table 2 [65-71]).

Furthermore, the more negative onset potential for Pd_{rNBH}/ZMO (= -0.99 V) in comparison with Pd_{rZHC}/ZMO (= -0.94 V), Pd_{rNBH} (= -0.95 V) and Pd_{rZHC} (= -0.93 V), specifying easier oxidation of HCHO on this electrocatalyst in comparison with other electrocatalysts. These better results for Pd_{rNBH}/ZMO against Pd_{rZHC}/ZMO are attributed to the nano size and great dispersion of palladium in the chemical reduction in contrast to the electrochemical system. In addition, the superior performance of Pd/ZMO compared to Pd electrocatalyst can be ascribed to two reasons. The large surface area and spongy structure of ZMO which it has led to providing a myriad of the active sites onto supported electrocatalysts. On the other hand, oxides containing transition metals have excellent oxygen storage capacity due to the transfer between their high and low valent [71]. Consequently, activates an oxidation-reduction cycle between (Mn^{7+}/ Mn^{6+}/ Mn^{5+}/ Mn^{4+}/ Mn^{3+}/ Mn^{2+}/ Mn^{1+}) in ZMO and the oxygen network, resistance to electrocatalyst poisoning.

Palladium, as a noble metal, is a beneficial electrocatalyst for the oxidation of single-carbon fuels. Still, as the reaction continues, the creation of a CO-like intermediate blocks the active site on the surface of the electrocatalyst. Hence, we can suggest a dual pathway for the HCHO oxidation on modified electrocatalysts in alkali. In the indirect electrochemical oxidation (A route), the formation of CO intermediate occurs. whereas direct HCHO oxidation into CO_2 by unstable intermediate (B rout) [72].

Based on the following eq. [73, 74] adsorbed hydroxyl onto the palladium surface can cause direct HCHO oxidation to CO_2 as its ending product. $Pd(CHO)_{ads}$ through pathways A and B can be directly turned into $Pd(CO)_{ads}$ and $Pd(COOH)_{ads}$. Route A creates CO_{ads} species, which has the role of an electron fouling intermediate, and $Pd(COOH)_{ads}$ oxidize to CO_2. The CO_{ads} can be desorbed from the surface to react with $Pd(OH)_{ads}$ oxidizing to CO_2.

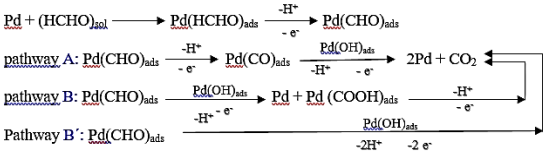

(8)

As shown in Reaction (5), in the first step, dehydrogenation released an electron and created an anodic peak at about 0.1 V. In this way, $Pd(CHO)_{ads}$ surface adsorbed species were produced. The surface adsorption of the intermediate species occupied the active sites of the electrocatalyst surface and led to an increase in the potential on the electrode surface. So, the release of subsequent electrons during hydrogenation (see Reaction (5)) created a shoulder of about 0.4 V.

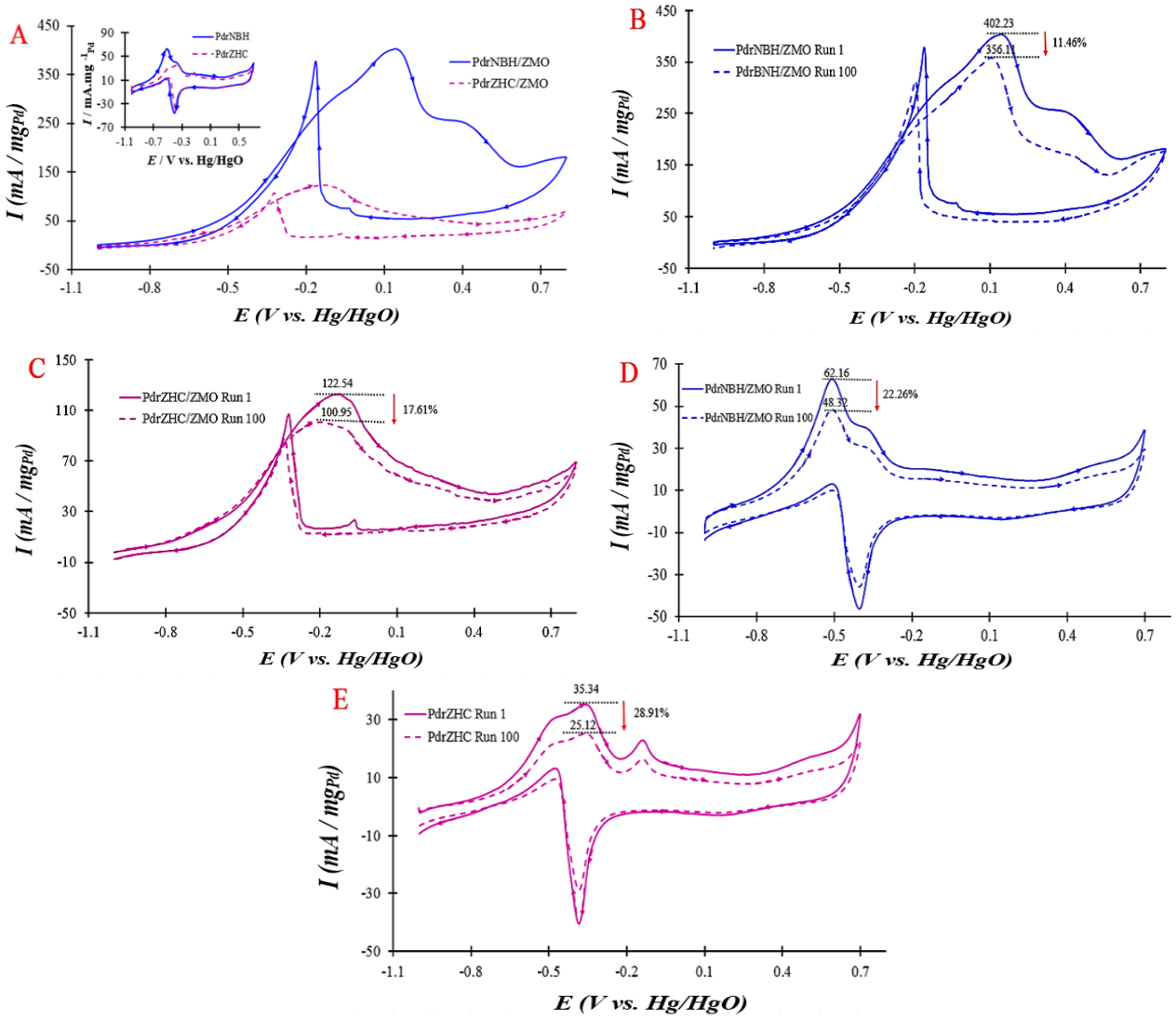

Fig. 4: (A) The comparing CV curves and (B), (C), (D), and (E) CV curves of the stability of peak current after 100 runs for the synthesized modified electrocatalysts in 1 M NaOH + 0.26 M HCHO solution from -1 to +0.7 V vs. Hg/HgO.

As well as the stability of peak currents after 100 runs was investigated by CV curves presented in Figs 4 (B), (C), (D), and (E) at the potential range of -1.0 to +0.7 V vs. Hg/HgO.

The current of forwarding peaks for 1st and 100th cycles were used for estimating the decay percentages for modified electrocatalysts. As clear in these Figures., The Pd_{rNBH}/ZMO and Pd_{rZHC}/ZMO electrocatalysts presented a lower decrease in initial current compared with support-less electrocatalysts. In addition, electrocatalysts manufactured with chemical reduction showed lower decay in initial current compared to the electrochemical reduction system.

Consequently, as a result of the more porous structure in supported electrocatalysts in contrast to support-less electrocatalysts and the small diameter and high dispersion during the chemical reduction in contrast to the electrochemical reduction system, the palladium nanoparticles were located in cavities, which can lessen the dissolution and accumulation of palladium.

The ChronoAmperometry (CA) analysis was done to explore the durability of the four modified electrocatalysts. Fig. 5 illustrates the CA plots at the voltage value at E = 0.1 V, in which the maximum current was acquired during 400 s.

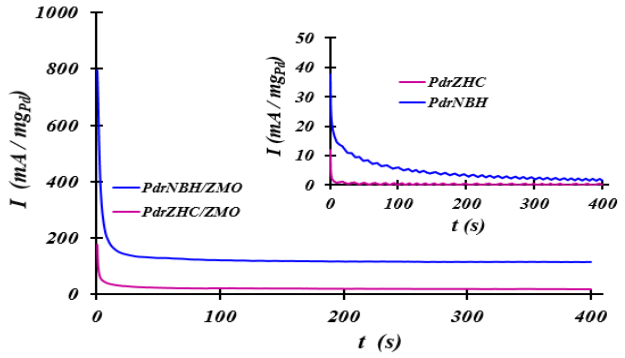

Fig. 5: The CA curves in the potential value at E = 0.1 V for the synthesized modified electrocatalysts in 1 M NaOH + 0.26 M HCHO solution

As clear, the oxidation currents speedily collapsed in the first seconds of CA curves. This decline is a result of blocking agents like hydrocarbons, oxygenates PdO_2, $Pd(OH)_4$, and CO [75].

As it is revealed in Fig. 5, the Pd_{rNBH}/ZMO has greater exchange current (=794.53 mA/mg_{Pd}) in comparison to the Pd_{rZHC}/ZMO (=175.48 mA/mg_{Pd}), Pd_{rNBH} (=37.68 mA/mg_{Pd}) and Pd_{rZHC} (=11.93 mA/mg_{Pd}) electrocatalyst. These data are in agreement with the CV's outcomes. In the cases of supported electrocatalysts (Pd_{rNBH}/ZMO and Pd_{rZHC}/ZMO), simultaneously with altering the surface potential, adsorbing media species like H_2 is accorded. As a result, the created oxygen network in the noble metal locality facilities removes the blocking electrocatalyst species produced during HCHO oxidation [22].

The HCHO number per catalyst surface per time is identified as the turnover number (TON) that defines the current in a steady state. It is calculated as [56]:

$$TON = \frac{J_{at\ 400\ s} \times N_A}{n \times F \times m_{Pd}} \quad (8)$$

Where J is the current density of steady state, n is the electrons transferred in electrooxidation of unique mole methanol, F is Faraday constant, $m_{Pd\ (111)}$ is $1.51 \times 10^{+15}$ atoms number/cm^2 and N_A is the Avogadro number. Also, the number of HCHO layers that are electro-oxidated per second is recognized as the TurnOver Frequency (TOF), follows as:

$$TOF = \frac{TON}{t} \quad (9)$$

TON = 3.76, 0.55, 0.05 and 0.08 – TOF = 6.26 $\times 10^{-3}$, 0.92 $\times 10^{-3}$, 0.09 $\times 10^{-3}$ and 0.14$\times 10^{-3}$ for Pd_{rNBH}/ZMO, Pd_{rZHC}/ZMO, Pd_{rNBH} and Pd_{rZHC} electrocatalysts respectively. The remarkable constancy may be owing to the enhanced formation of OH species and their reaction with CO on the $Pd_{rNBH\ or\ rZHC}$/ZMO surface.

CONCLUSIONS

Decorating Pd on spinel ZMO micro-sponge as the support was done with two different chemical and electrochemical reduction scenarios. The palladium in chemical reductions (Pd_{rNBH}/ZMO) illustrated a smaller particle size and higher dispersion than the electrochemical (Pd_{rZHC}/ZMO) system. The more voltage of the cell in chemical procedure than the electrochemical system causes big changes in Gibbs free energy. To study the performance of electrocatalysts, the EAS was measured and compared with non-supported Pd electrocatalysts. The EAS values for modified electrodes were improved by applying for ZMO support. The EAS for Pd_{rNBH}/ZMO was 4.89 times larger than Pd_{rZHC}/ZMO. The ability of HCHO oxidation in modified electrocatalysts (current = 420.89 mA.mg Pd^{-1} for Pd_{rNBH}/ZMO and 120.21 mA/mg_{Pd} for Pd_{rZHC}/ZMO) was much better than Pd electrocatalysts (current =35.23 mA/mg_{Pd} for Pd_{rNBH} and 21.13 mA/mg_{Pd} for Pd_{rZHC}). Comparing electrocatalysts demonstrated the multi-oxidative states of ZMO may be a promoter agent for the dehydrogenation as the initial step of oxidation of HCOH. Also, the porous ZMO structure is subjected to prevent Pd aggregation.

Acknowledgments

This research was supported by the University of Sistan and Baluchestan.

Received : Oct. 30, 2022 ; Accepted : Jan.30, 2023

REFERENCES

[1] Trafela Š., Zavašnik J., Šturm S., Rožman K.Z., Formation of a $Ni(OH)_2$/NiOOH Active Redox Couple on Nickel Nanowires for Formaldehyde Detection in Alkaline Media, *Electrochimica Acta*, **30(444)**: 346-353 (2019).

[2] Yi Q., Niu F., Yu W., Pd-Modified TiO_2 Electrode for Electrochemical Oxidation of Hydrazine, Formaldehyde and Glucose, *Thin Solid Films*, **519(10):** 3155-3161(2011).

[3] He F. G., Du B., Sharma G., Stadler F. J., Highly Efficient Polydopamine-Coated Poly(Methylmethacrylate) Nanofiber Supported Platinum–Nickel Bimetallic Catalyst for Formaldehyde Oxidation at Room Temperature, *Polymers*, **11(4)**: 674-688 (2019).

[4] Ji J., Lu X., Chen Ch., He M., Huang H., Potassium-Modulatedδ-MnO_2 as Robust Catalysts for Formaldehyde Oxidation at Room Temperature, *Applied Catalysis B: Environmental*, **260(1)**: 118210-18222 (2020).

[5] O'Sullivan E.J.M, White J.R., Electro-Oxidation of Formaldehyde on Thermally Prepared ruo_2 and Other Noble Metal Oxides, *Journal of the Electrochemical Society*, **136(9)**: 2576-2583 (1989).

[6] Geng J., Bi Y., Lu G., Morphology-Dependent Activity of Silver Nanostructures Towards the Electro-Oxidation of Formaldehyde, *Electrochemistry Communications*, **11(6)**: 1255–1258 (2009).

[7] Abrishamkar M., Barootkoob M., Electrooxidation of Formaldehyde as a Fuel for Fuel Cells Using Fe^{2+}-Nano-Zeolite Modified Carbon Paste Electrode, *International Journal of Hydrogen Energy*, **42(37)**: 23821-23825 (2017).

[8] Dong Q., Li Y., Zhu L., Ma T., Guo C., Electrocatalytic Oxidation of Methanol and Formaldehyde on Platinum-Modified Poly(o-Methoxyaniline)-Multiwalled Carbon Nanotube Composites, *International Journal of electrochemical science*, **8(7)**: 8191-8200 (2013).

[9] Luo K., Wang H., Li X., Electrocatalytic Activity of Ligand-Protected Gold Particles: Formaldehyde Oxidation, *Gold Bulletin*, **47(1)**: 41-46 (2014).

[10] Biuck H., Serveh G.h., Electrooxidation of Formic Acid and Formaldehyde on the Fe_3O_4@Pt Core-Shell Nanoparticles/Carbon-Ceramic Electrode, *Iranian Journal of Chemistry and Chemical Engineering*, **35(4)**: 99-112 (2016).

[11] Gao G., Guo D., Li H., Electrocatalytic Oxidation of Formaldehyde on Palladium Nanoparticles Supported on Multi-Walled Carbon Nanotubes, *Journal of Power Sources*, **162(2)**: 1094-1098 (2006).

[12] Safavi A., Maleki N., Farjami F., Farjami E., Electrocatalytic Oxidation of Formaldehyde on Palladium Nanoparticles Electrodeposited on Carbon Ionic Liquid Composite Electrode, *Journal of Electroanalytical Chemistry*, **626(1-2)**: 75–79 (2009).

[13] Vaskelis A., Tarozaite R., Jagminiene A., Tamasauskaite Tamasiunaite L., Juskenas R., Kurtinaitiene M., Gold Nanoparticles Obtained by Au(III) Reduction with Sn(II): Preparation and Electrocatalytic properties in Oxidation of Reducing Agents, *Electrochimica Acta*, **53(2)**: 407–416 (2007).

[14] Selvaraj V., Alagar M., Sathish Kumar K., Synthesis and Characterization of Metal Nanoparticles-Decorated PPY–CNT Composite and Their Electrocatalytic Oxidation of Formic Acid and Formaldehyde for Fuel Cell Applications, *Applied Catalysis, B: Environmental*, **75(1-2)**: 129–138 (2007).

[15] Hassaninejad–Darzi S.K., A novel, Effective and Low Cost Catalyst for Formaldehyde Electrooxidation Based on Nickel Ions Dispersed Onto Chitosan-Modified Carbon Paste Electrode for Fuel Cell, *Journal of Electroceramics*, **33(1)**: 252–263 (2014).

[16] Jahan-Bakhsh R., Ojani R., Abdi S., Hosseini S. R., Highly Improved Electrooxidation of Formaldehyde on Nickel/poly (O-Toluidine)/Triton X-100 Film Modified Carbon Nanotube Paste Electrode, *International Journal of Hydrogen Energy*, **37(3)**: 2137-2146 (2012).

[17] Ojani R., Jahan-Bakhsh R., Ahmady-Khanghah Y., Safshekan S., Copper-poly (2-Aminodiphenylamine) Composite as Catalyst for Electrocatalytic Oxidation of Formaldehyde in Alkaline Media, *International Journal of Hydrogen Energy*, **38(13)**: 5457-463 (2013).

[18] Behbahani E. S., Eshghi A., Ghaedi M., Bimetallic PtPd Nanoparticles Relying on $CoNiO_2$ and Reduced Graphene Oxide as a Most Operative Electrocatalyst Toward Ethanol Fuel Oxidation, *International Journal of Hydrogen Energy*, **4(49)**: 24977-24990 (2021).

[19] Siwal S., Matseke S., Mpelane S., Hooda N., Nandi D., Mallick K., Palladium-Polymer Nanocomposite: An Anode Catalyst for the Electrochemical Oxidation of Methanol, *International Journal of Hydrogen Energy*, **42(37)**: 23599-23605 (2017).

[20] Altuner E.E., Ozalp V.C., Yilmaz M.D., Sudagidan M., Aygun A., Acar E.E., Tasbasi B. B., Sen F., Development of Electrochemical Aptasensors Detecting Phosphate Ions on TMB Substrate with Epoxy-Based Mesoporous Silica Nanoparticles, *Chemosphere*, **297(1)**: 134077 (2022).

[21] Selvaraj V., Nirmala Grace A., Alagar M., Electrocatalytic Oxidation of Formic Acid and Formaldehyde on Nanoparticle Decorated Single Walled Carbon Nanotubes, *Journal of Colloid and Interface Science*, **333(1)**: 254–262 (2009).

[22] Yavari Z., Noroozifar M., Mirghoreishi Roodbaneh, M., Ajorlou, B., $SrFeO_{3-\delta}$ Assisting with Pd Nanoparticles on the Performance of Alcohols Catalytic Oxidation, *Iranian Journal of Chemistry and Chemical Engineering (IJCCE)*, **36(6)**: 21-37 (2017).

[23] Fedoseev I.V., Shevelkov A.V., Vasekin V.V., Poyarkov K.B., Rovinskaya N.V., Formation and Destruction of Palladium Carbonyl Nanoclusters in the Pd(II)–Cl—H+–H_2O–CO Systems, *Russian Journal of Inorganic Chemistry*, **65(1)**:161–168 (2020).

[24] Klein M., Nadolna J., Gołąbiewska A., Mazierski P., Klimczuk T., Remita H., Zaleska-Medynskam A., The Effect of Metal Cluster Deposition Route on Structure and Photocatalytic Activity of Mono- and Bimetallic Nanoparticles Supported on TiO_2 by Radiolytic Method, *Applied Surface Science*, **378**: 37-48 (2016).

[25] Sunagawa Y., Yamamoto K., Takahashi H., Muramatsu A., Liquid-Phase Reductive Deposition as a Novel Nanoparticle Synthesis Method and Its Application to Supported Noble Metal Catalyst Preparation, *Catalysis Today*, **132(1-4)**: 81–87 (2008).

[26] Altuner E.E., Gur T., 10 - Ternary/quaternary Nanomaterials for Direct Alcohol Fuel Cells, Nanomaterials for Direct Alcohol Fuel Cells: Characterization, Design, and Electrocatalysis, F. Şen (Ed.) Micro and Nano Technologies, *Elsevier*, 157-172 (2021).

[27] Eshghi A., Kheirmand M., Electroplating of Pt–Ni–Cu Nanoparticles on Glassy Carbon Electrode for Glucose Electro-Oxidation Process, *Surface Engineering*, **35(2)**:128-134 (2019).

[28] Kuppan B., Selvam P., Platinum-Supported Mesoporous Carbon (Pt/CMK-3) as Anodic Catalyst for Direct Methanol Fuel Cell Applications: The Effect of Preparation and Deposition Methods, *Progress in Natural Science: Materials International*, **22(6)**: 616-623 (2012).

[29] Gomroki S., Yavari Z., Abbasian A.R., Shafiee Afarani M., Noroozifar M., Stabilizing Nano-Pd on Porous Li_2TiO_3 *via* Chemical and Electrochemical Reduction Systems for the Electrooxidation of Ethylene Glycol, *Materials Chemistry and Physics*, **281(1)**: 125896-125905 (2022).

[30] Xie X., Li Y., Liu Zh. Q., Haruta M., Shen W., Low-Temperature Oxidation of CO Catalysed by Co_3O_4 Nanorods, *Nature*, **458(7239)**: 746-749 (2009).

[31] Hu L., Peng Q., Li Y., Selective Synthesis of Co_3O_4 Nanocrystal with Different Shape and Crystal Plane Effect on Catalytic Property for Methane Combustion, *Journal of the American Chemical Society*, **130(48)**: 16136-16137 (2008).

[32] Zhang K., Yang W., Ma Ch., Wang Y., Sun Ch., Chen Y., Duchesne P., Zhou J., Wang J., Hu Y., Banis M.N., Zhang P., Li F., Li J., Chen L., A Highly Active, Stable and Synergistic Pt Nanoparticles/Mo_2C Nanotube Catalyst for Methanol Electro-Oxidation, *NPG Asia Materials*, **7(1)**: 153-163 (2015).

[33] Barakat N.A.M., Abdelkareem M.A., El-Newehy M., Kim H.Y., Influence of the Nanofibrous Morphology on the Catalytic Activity of NiO Nanostructures: an Effective Impact Toward Methanol Electrooxidation, *Nanoscale Research Letters*, **8(1)**: 1-6 (2013)

[34] Kua J., A. Goddard W., Oxidation of Methanol on 2nd and 3rd Row Group VIII Transition Metals (Pt, Ir, Os, Pd, Rh, and Ru): Application to Direct Methanol Fuel Cells, *Journal of the American Chemical Society*, **121(47)**: 10928–10941(1999).

[35] Li Y., Tang L., Deng D., Ye J., Wu Zh., Wang J., Luo L., A Novel Non-Enzymatic H_2O_2 Sensor Using Znmn2o4 Microspheres Modified Glassy Carbon Electrode, *Colloids and Surfaces B: Biointerfaces*, **179(1)**: 293–298 (2019).

[36] Luo X., Zhang X., Chen L., Li L., Zhu G., Chen G., Yan D., Xu H., Yu A., Mesoporous $ZnMn_2O_4$ Microtubules Derived from a Biomorphic Strategy for High Performance Lithium/Sodium Ion Batteries, *ACS Applied Materials & Interfaces*, **10(39)**: 33170–33178 (2018).

[37] Courtel F.M., Abu-Lebdeh Y., Davidson I.J., $ZnMn_2O_4$ Nanoparticles Synthesized by a Hydrothermal Method as an Anode Material for Li-Ion Batteries, *Electrochimica Acta*, **71**: 123–127 (2012).

[38] Lobo L.S., Kumar A.R., Investigation of Structural and Electrical Properties of $ZnMn_2O_4$ Synthesized by Sol–Gel Method, *Journal of Materials Science: Materials in Electronic*, **27(1)**: 7398–7406 (2016).

[39] Bessekhouad Y., Trari M., Photocatalytic Hydrogen Production from Suspension of Spinel Powders AMn_2O_4 (A=Cu and Zn), *International Journal of Hydrogen Energy*, **27(4)**: 357–362 (2002).

[40] Zhao L., Li X., Zhao J., Fabrication, Characterization and Photocatalytic Activity of Cubic-Like $ZnMn_2O_4$, *Applied Surface Science*, **268**: 274–277 (2013).

[41] Courtel F.M., Duncan H., Abu-Lebdeh Y., Davidson I.J., High Capacity Anode Materials for Li-Ion Batteries Based on Spinel Metal Oxides AMn_2O_4 (A = Co, Ni, and Zn), *Journal of Materials Chemistry*, **21(27):**10206-10218 (2011).

[42] Yang Y., Zhao Y., Xiao L., Zhang L., Nanocrystalline $ZnMn_2O_4$ as A Novel Lithium-Storage Material, *Electrochemistry communications*, **10(8)**: 1117–1120 (2008).

[43] Gupta M., Gupta M., Anu, Mudsainiyan R.K., Randhawa B.S., Physico-Chemical Analysis of Pure and Zn Doped Cd Ferrites ($Cd_{1-x}Zn_xFe_2O_4$) Nanofabricated by Pechini Sol–Gel Method, *Journal of Analytical and Applied Pyrolysis*, **116**: 75–85 (2015).

[44] Gharibshahian M., Nourbakhsh M.S., Mirzaee O., Evaluation of the Superparamagnetic and Biological Properties of Microwave Assisted Synthesized Zn & Cd Doped $CoFe_2O_4$ Nanoparticles Via Pechini Sol–Gel Method, *Journal of Sol-Gel Science and Technology*, **85**: 684-692 (2018).

[45] Vlazan P., Stoia M., Structural and Magnetic Properties of $CoFe_2O_4$ Nanopowders, Prepared Using a Modified Pechini Method, *Ceramics International*, **44(1)**: 530–536 (2018).

[46] Motavallian P., Abasht B., Abdollah-Pour H., Zr Doping Dependence of Structural and Magnetic Properties of Cobalt Ferrite Synthesized by Sol–Gel Based Pechini Method, *Journal of Magnetism and Magnetic Materials*, **451**: 577–586 (2018).

[47] Tan Q., Zhu H., Guo Sh., Chen Y., Jiang T., Shu Ch., Chong Sh., Hultman B., Liu Y., Wu G., Quasi-Zero-Dimensional Cobalt Doped CeO_2 Dots on Pd Catalysts for Alcohol Electro-Oxidation with Enhanced Poisoning-Tolerance, *Nanoscale*, **9(34)**: 12565-72 (2017).

[48] E. Altuner E., Ozalp V. C., Yilmaz M D, Bekmezci M., Sen F., High-Efficiency Application of CTS-Co NPs Mimicking Peroxidase Enzyme on TMB(ox), *Chemosphere*, **292**: 133429 (2022).

[49] Abbasian A.R., Shafiee Afarani M., One-Step Solution Combustion Synthesis and Characterization of $ZnFe_2O_4$ and $ZnFe_{1.6}O_4$ Nanoparticles, *Applied Physics A*, **125 (721)**: 1-12 (2019).

[50] Abbasian A.R., Rahmani M., Salt-Assisted Solution Combustion Synthesis of Nanostructured $ZnFe_2O_4$-ZnS Powders, *Inorganic Chemistry Communications*, **111**: 107629-51 (2020).

[51] Eshghi A., Sabzehmeidani M.M., Platinum–Iron Nanoparticles Supported on Reduced Graphene Oxide as an Improved Catalyst for Methanol Electro Oxidation, *International Journal of Hydrogen Energy*, **43(12)**: 6107-6116 (2018).

[52] Yavari Z., Noroozifar M., Parvizi T., Performance Evaluation of Anodic Nano-Catalyst for Direct Methanol Alkaline Fuel Cell, *Environmental Progress & Sustainable Energy*, **37(1)**: 597-604 (2018).

[53] Habibi B., Aluminum Supported Palladium Nanoparticles: Preparation, Characterization and Application for Formic Acid Electrooxidation, *International Journal of Hydrogen Energy*, **38(13)**: 5464–5473 (2013).

[54] Li Sh., Shu J., Ma S., lei H., Jin Y. J., Zhang X., Jin R., Engineering Three-Dimensional Nitrogen-Doped Carbon Black Embedding Nitrogen Doped Graphene Anchoring Ultrafine Surface Clean Pd Nanoparticles as Efficient Ethanol Oxidation Electrocatalyst, *Applied Catalysis B: Environmental*, **280**: 119464-119473 (2021).

[55] Kaedi F., Yavari Z., Noroozifar M., Saravani H., Promoted Electrocatalytic Ability of the Pd on Doped Pt in NiOMgO Solid Solution Toward Methanol and Ethanol Oxidation, *Journal of Electroanalytical Chemistry*, **827**: 204-212 (2018).

[56] Qiu X., Zhang H., Wu P., Zhang F., Wei S., Sun D., Xu L., Tang Y., One-Pot Synthesis of Freestanding Porous Palladium Nanosheets as Highly Efficient Electrocatalysts for Formic Acid Oxidation, *Advanced Functional Materials*, **27(1)**: 1603852-61 (2016).

[57] Singh R.N., Singh A., Anindita, Electrocatalytic Activity of Binary and Ternary Composite Films of Pd, MWCNT and Ni, Part II: Methanol Electrooxidation in 1 M KOH, *International Journal of Hydrogen Energy*, **34(1)**: 2052 – 2057 (2009).

[58] Kiyani R., Parnian MJ., Rowshanzamir S., Investigation of the Effect of Carbonaceous Supports on the Activity and Stability of Supported Palladium Catalysts for Methanol Electrooxidation Reaction, *International Journal of Hydrogen Energy*, **42(36)**: 2070-23084 (2017).

[59] Wang X., Tang B., Huang X., Ma Y., Zhang Zh., High Activity of Novel Nanoporous Pd–Au Catalyst for Methanol Electro-Oxidation in Alkaline Media, *Journal of Alloys and Compounds*, **565:**120–126 (2013).

[60] Li R., Hao H., Cai W-B, Huang T., Yu A., Preparation of Carbon Supported Pd–Pb Hollow Nanospheres and their Electrocatalytic Activities for Formic Acid Oxidation, *Electrochemistry Communications*, **12(7):** 901–904 (2010).

[61] Arjona N., Rivas S., Álvarez-Contreras L., Guerra-Balcazar M., Ledesma-Garcı J., Kjeangd E., Arriaga L. G., Glycerol Electro-Oxidation in Alkaline Media Using Pt and Pd Catalysts Electrodeposited on Three-Dimensional Porous Carbon Electrodes, *New Journal of Chemistry*, **41(4)**: 1854-1863 (2017).

[62] Huang Y., Yin M., Zhou X., Liu Ch., Xing W., Formation of Porous Pd Black Induced by in Situ catalytic Reaction, *Nanotechnology*, **23(3)**: 035605-11 (2012).

[63] Qadir K., Joo S. H., Mun B. S., Butcher D. R., Renzas J. R., Aksoy F., Liu Zh., Somorjai G. A., Park J. Y., Intrinsic Relation Between Catalytic Activity of CO Oxidation on Ru Nanoparticles and Ru Oxides Uncovered with Ambient Pressure XPS, *Nano letters*, **12(11)**: 5761–5768 (2012).

[64] Zhang Y., Cao Y., Chen D., Cui P., Yang J., Ionic Liquid Assisted Synthesis of Palladium Nanoclusters for Highly Efficient Formaldehyde Oxidation, *Electrochimica Acta*, **269:** 38-44 (2018).

[65] Ojani R., Raoof J-B, Safshekan S., Photoinduced Deposition of Palladium Nanoparticles On TiO_2 Nanotube Electrode and Investigation of Its Capability for Formaldehyde Oxidation, *Electrochimica Acta*, **138(1)**: 468–475 (2014).

[66] Ejaz A., Ahmed M.S., Jeon S., Synergistic Effect of 1,4-Benzenedimethaneamine Assembled Graphene Supported Palladium for Formaldehyde Oxidation Reaction in Alkaline Media, *Journal of the Electrochemical Society*, **163(5)**: B163–B168 (2016).

[67] Li Z., Lu Z.X., Li B., Bai L., Wang Q., Research on Electrochemical Oxidation of Formaldehyde on the Nanoporous Silver Electrode in Alkaline Solution, *ECS Electrochemistry Letters*, **4(6):** H24–H27 (2015).

[68] Bansal V., Li V., Mullane A.P.O., Bhargava S.K., Shape Dependent Electrocatalytic Behavior of Silver Nanoparticles, *Cryst. Eng. Comm.*, **12(12):** 4280–4286 (2010).

[69] Li H., Zhang Y., Wan Q., Li Y., Yang N., Expanded Graphite and Carbon Nanotube Supported Palladium Nanoparticles for Electrocatalytic Oxidation of Liquid Fuels, *Carbon*, **131(1)**: 111-119 (2018).

[70] Gorle D.B., Kulandainathan M.A., One-pot Synthesis of Highly Efficient Graphene Based Three-Dimensional Hybrids as Catalyst Supporting Materials for Electro-Oxidation of Liquid Fuels, *Journal of Materials Chemistry A*, **5(29)**: 15273-15286 (2017).

[71] Cao J. L., Shao G. S., Ma T. Y., Wang Y., Ren T. Zh., Wu Sh. H., Yuan Zh. Y., Hierarchical Meso–Macroporous Titania-Supported CuO Nanocatalysts: Preparation, Characterization and Catalytic CO Oxidation, *Journal of Materials Science*, **44**: 6717–6726 (2009).

[72] Teixeira L.S.G., Leão E.S., Dantas A. F., Pinheiro H.L.C., Costa A. C.S., Andrade J. B.de, Determination of Formaldehyde in Brazilian alcohol Fuels by Flow-Injection Solid Phase Spectrophotometry, *Talanta*, **64(3)**: 711-715 (2004).

[73] Saleh Ahammad A.J., Shaikh A.A., Jessy N.J., Tania Akter, Abdullah Al Mamun, P.K. Bakshi, Hydrogen Peroxide Biosensor based on the Immobilization of Horseradish Peroxidase onto a Gold Nanoparticles-Adsorbed Poly (Brilliant Cresyl Blue) Film, *Journal of the Electrochemical Society*, **162(3):** B52-B56(2015).

[74] Correia A.N., Mascaro L.H., Machado S.A.S., Avaca L.A., Amorphous Palladium-Silicon Alloys for the Oxidation of Formic Acid and Formaldehyde. A Voltammetric Investigation, *Journal of the Brazilian Chemical Society*, **10**: 478-482 (1999).

[75] Eris S., Das_Delen Z., Sen F., Enhanced Electrocatalytic Activity and Stability of Monodisperse Pt Nanocomposites for Direct Methanol Fuel Cells, *Journal of Colloid and Interface Science*, **513(1)**: 767–773 (2018).